Organic & Biomolecular Chemistry

ROYAL SOCIETY OF CHEMISTRY

PAPER

View Article Online
View Journal | View Issue

Check for updates

Cite this: *Org. Biomol. Chem.*, 2023, **21**, 2968

Fluorescent sensing of non-steroidal anti-inflammatory drugs naproxen and ketoprofen by dansylated squaramide-based receptors†

Giacomo Picci, [a] M. Carla Aragoni, [a] Massimiliano Arca, [a] Claudia Caltagirone, *[a] Mauro Formica, [b] Vieri Fusi, *[b] Luca Giorgi, [b] Filippo Ingargiola,[c] Vito Lippolis, [a] Eleonora Macedi, [b] Luca Mancini, [b] Liviana Mummolo[c] and Luca Prodi *[c]

Received 28th February 2023,
Accepted 12th March 2023

DOI: 10.1039/d3ob00324h

rsc.li/obc

Bis-squaramide receptors **L1–L4** bearing a dansyl moiety were synthesised and their potential applications as fluorescent probes towards non steroidal anti-inflammatory drugs naproxen and ketoprofen was investigated. A detailed photophysical characterization in CH_3CN/DMSO solution (9 : 1 v/v) was conducted and demonstrated that the two macrocyclic receptors **L1** and **L2** show good sensitivity towards ketoprofen with an ON–OFF fluorescent response, while the two open chain receptors **L3** and **L4** behave similarly with the three guests considered. DFT theoretical calculations carried out on **L2** and **L4** as model receptors allowed to propose a possible coordination mode towards the guests. Finally, ^{1}H-NMR spectroscopy in DMSO-d_6/0.5% water solution demonstrated that the four receptors interact with the considered guests *via* H-bonds.

Introduction

Environmental water pollution is today a fundamental issue in the control and safeguard of the public health because water is of crucial importance for life sustainability. The problem is becoming more and more urgent due to the continuously increasing number of chemicals released into the environment, which makes the bunch of compounds with potential ecological and toxicological risk enormous. Among the chemicals present in environmental water, emerging pollutants (EPs) are of particular interest because they are not routinely monitored. EPs are defined as "*synthetic or naturally occurring chemicals or any microorganisms that are not commonly monitored in the environment but have the potential to enter the environment and cause known or suspected adverse ecological and/or human health effects*".[1] For some of them the potential lethal impact on human and wildlife endocrine systems is already known, even when present at trace quantities.[2] EPs listed in European aquatic environments account for about 700 compounds divided into 20 categories, the most representative being pharmaceuticals, personal care products, endocrine disrupting chemicals (EDCs), hormones and steroids, perfluorinated compounds (PFCs), surfactants, flame retardants, plasticizers, industrial and fuel additives, and antiseptics.[3]

Among pharmaceuticals, anti-inflammatory drugs are well represented in the EPs list. In particular, non-steroidal anti-inflammatory drugs (NSAIDs) represent a real threat for the environment for their ubiquitous occurrence in water worldwide and the resultant environmental implications in aquatic ecosystems.[4] Among NSAIDs, naproxen (NPX)[5] and ketoprofen (KET)[6] are particularly interesting due to their massive consumption and different strategies for their removal have been proposed, such as bacterial degradation, photo-degradation or absorption on zeolites.[5] NPX and KET present a carboxylic acid moiety that can be easily deprotonated. Indeed, they are mostly commercialized in their anionic form as sodium or lysine salts. These chemicals are currently determined by off-site analysis that require collection, transportation, eventual pre-treating of the sample, and expensive instrumentations such as high-performance liquid chromatography (HPLC), gas-chromatography with different detection end-units, and specifically trained staff. Thus, providing devices able to allow a rapid on-site detection of target analytes would have a dramatic impact on the environmental control with significant economic benefits.[7] The development of chemical sensors has been conceived to bypass restrictions related to classical analytical protocols and use of conventional laboratory tech-

[a]*Dipartimento di Scienze Chimiche e Geologiche, Università degli Studi di Cagliari, S.S. 554 Bivio per Sestu, 09042 Monserrato, CA, Italy. E-mail: ccaltagirone@unica.it*
[b]*Department of Pure and Applied Science, University of Urbino, Via della Stazione 4, I-61029 Urbino, Italy. E-mail: vieri.fusi@uniurb.it*
[c]*Department of Chemistry "Giacomo Ciamician", Università degli Studi di Bologna, Via Selmi 2, 40126 Bologna, Italy. E-mail: luca.prodi@unibo.it*

†Electronic supplementary information (ESI) available. See DOI: https://doi.org/10.1039/d3ob00324h

niques for environmental control. While the technologic foundation for chemical sensors already exists, their application to EPs detection is complicated by the difficulty in the design of selective receptors due to the large number and diversity of listed EPs.[8] Ideally, a receptor able to bind NPX and KET in their anionic forms should include strong hydrogen bond (HB) donors to interact with the carboxylate moiety and an aromatic portion able to interact with the aromatic rings of the drugs *via* hydrophobic or π-stacking interactions.[9,10]

Among HB donor scaffolds, one of the most efficient is squaramide (3,4-diamino-3-cyclobuten-1,2-dione derivatives), that is a well-studied four membered aromatic unit with interesting chemical and physical properties.[11] The applications of squaramide derivatives range across a wide variety of chemistry fields from medicinal chemistry to biochemistry, from material science to organometallic chemistry, from organocatalysis to molecular recognition.[12] Indeed, the possibility to act as both H-bond donor and acceptor, the structural rigidity, aromaticity, as well as the ability to form bi-directional hydrogen bonds confer them unique properties in binding anion species, such as halogens and carboxylates.[11,12] Costa, Ballester and co-workers proved that tailored squaramides can be used as binding subunits for carboxylates sensing and recognition in polar hydrophilic competitive media.[13,14] Moreover, recent studies established that the increase in aromaticity upon HB formation represents the primary driving force to bind anions forming stable adducts, and justifies the extensive use of the squaramide scaffold in the design of receptors and chemosensors.[15–17] In addition, the coupling of two squaramide moieties in a macrocyclic framework reinforces the anion binding properties of the receptor, allowing to bind inorganic oxa-anions in water with selectivity depending on the pH.[18–20] However, to the best of our knowledge, squaramide-based receptors have never been exploited for NSAIDs recognition.

Starting from these considerations, we report here four new dansylated squaramide-based receptors (**L1–L4**, Fig. 1) for the binding and sensing of NPX and KET in organic media. Each receptor contains two squaramide units connected *via* a dipropylenamine spacer bearing a dansyl group as fluorescent signaling unit linked to the central nitrogen atom. The four receptors show different structural features: **L1** and **L2** have a macrocyclic topology, whereas **L3** and **L4** are open-chain receptors in which the two terminal squaramide units are connected either to two benzyl groups to increase the area of hydrophobic interaction (**L3**) or two indole rings to increase the number of HB donor sites (**L4**). The non-fluorescent receptor **L5**, reported in Fig. 1, showing the same macrocyclic topology as **L1** has been studied for the sake of comparison. This study aims at understanding how and to which extent the molecular topology and the number of HB donors of these bis-squaramide receptors may influence the selectivity and the signaling efficiency towards the selected targets analytes NPX and KET in their anionic forms (NPX^- and KET^-, respectively, Fig. 1). Benzoate (BzO^-, Fig. 1) was also considered for the sake of comparison.

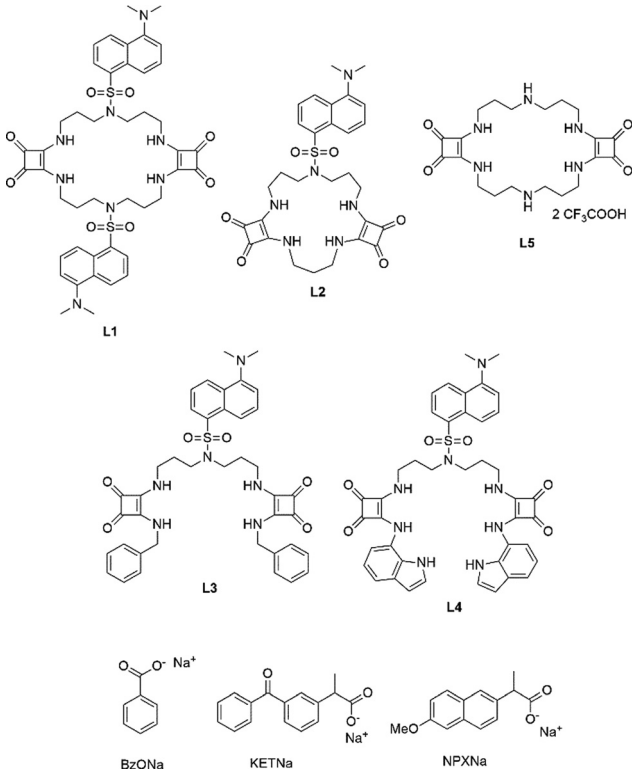

Fig. 1 Receptors **L1–L5** discussed in the paper and targets as their sodium salts.

Results and discussion

Synthesis

The synthetic strategy adopted to obtain receptors **L1–L5** is outlined in the ESI, Scheme S1.† The key intermediate **4** was synthesized starting from dansyl chloride **1** and *N*,*N*-bis(3-trifluoroacetylaminopropyl)ammonium trifluoroacetate **2**, synthesized as reported in the literature,[21] and subsequent deacetylation of the primary amine functions under basic methanolic conditions. Intermediate **4** was converted into its bis-ethoxysquaramide derivative **6** by following a coupling reaction with two equivalents of diethylsquarate **5**. Macrocyclic systems **L1** and **L2** were obtained in good yields by a modified high-dilution Richman–Atkins cyclization[22] using **6** as electrophilic difunctional intermediate and diamines **4** or **7**, respectively, as nucleophilic reagents. Open chain receptor **L3** was obtained by direct coupling of the intermediate **6** with two equivalents of benzylamine **8** in ethanol at room temperature. Due to the lower reactivity of aromatic amines, the receptor **L4** was obtained in two steps: (i) coupling of the diethylsquarate **5** with the 7-aminoindole **9** in the presence of a catalytical amount of zinc triflate, and subsequently (ii) reaction of the intermediate **10** with **4**, in hot ethanol in the presence of zinc triflate. All receptors precipitated from the reaction mixture. **L1–L3** were purified in acceptable yields by crystallization from hot concentrated DMF solutions (see ESI for synthetic details, ^{1}H-, ^{13}C-NMR spectra, Fig. S1–S11†).

Photophysical characterization

A detailed photophysical characterization was carried out on **L1–L5** and their ability to bind and sense BzO^-, KET^- and NPX^- as their sodium salts was evaluated.‡ The scarce solubility of **L1–L5** in water prevented spectrophotometric and spectrofluorimetric studies in this solvent and in aqueous mixtures. Preliminary spectrophotometric and spectrofluorimetric studies were conducted on **L1–L5** in DMSO. As reported in Fig. S12 and S13 in the ESI,† in the case of **L4** no significant changes in the absorption and the emission spectra were observed upon the addition of increasing amounts of NPX^- and KET^-. Similar results were obtained for the other receptors. In order to enhance the optical response of **L1–L5**, we decided to conduct the measurements in a less competitive medium, *i.e.* CH_3CN/DMSO solution (9 : 1 v/v). The absorption spectrum in CH_3CN/DMSO solution (9 : 1 v/v) of **L5** containing two squaramide units shows an intense band (ε = 51 000 $M^{-1}cm^{-1}$) centred at 285 nm. In the case of **L1**, **L2**, and **L3**, a shoulder is present in the 310–340 nm region, where the dansyl chromophore absorbs (the dansylamide showing a maximum at 330 nm with a ε = 3800 M^{-1} cm^{-1}). As expected, the absorption spectra of these receptors are very similar to the sum of spectra of **L5** and one (**L2** and **L3**) or two (**L1**) dansyl units. In the absorption spectrum of **L4**, the band of the squaramide is strongly perturbed by the nearby indole units, with the maximum being red-shifted to 335 nm – as supported by the theoretical calculations reported below – in coincidence with the maximum of the dansyl unit; the total absorption coefficient at this wavelength is ε = 30 500 M^{-1} cm^{-1} (Fig. 2).

As far as the emission spectra are concerned, at room temperature in CH_3CN/DMSO solution (9 : 1 v/v) **L5** does not show any fluorescence, while **L1** (Φ = 0.77; τ = 13,2 ns), **L2** (Φ = 0.77; τ = 12,6 ns), **L3** (Φ = 0.75; τ = 13,7 ns), and **L4** (Φ = 0.095; τ = 11,3 ns), as shown in Fig. 3, display the typical fluorescence band at 525 nm of the dansyl chromophore under the same experimental conditions, as it can be observed for the dansylamide (λ_{max} = 510 nm, Φ = 0.88; τ = 12.9 ns). In all cases when at least a dansyl unit is present, the shape of the corrected excitation spectrum is similar to that of the absorption spectrum of the dansylamide. On the contrary, the contribution attributable to the squaramides is almost completely absent, indicating that no energy transfer from these units to the dansyl moiety occurs. The absence of energy transfer between the chromophoric units in the receptor can also explain the lower quantum yield observed for **L4**, since in this case the contribution of the dansyl unit to the absorption at 330 nm (the excitation at which the quantum yield has been measured) can be estimated to be only 12%, the 88% being absorbed by the indole units.

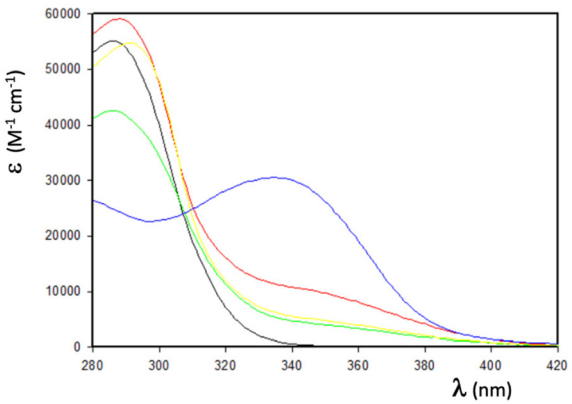

Fig. 2 Absorption spectra in CH_3CN/DMSO solution (9 : 1 v/v) of the hosts **L5** (black), **L1** (red), **L2** (green), **L3** (yellow), and **L4** (blue).

‡A note on the role of the counter-cation in the spectroscopic measurements is reported in ESI.†

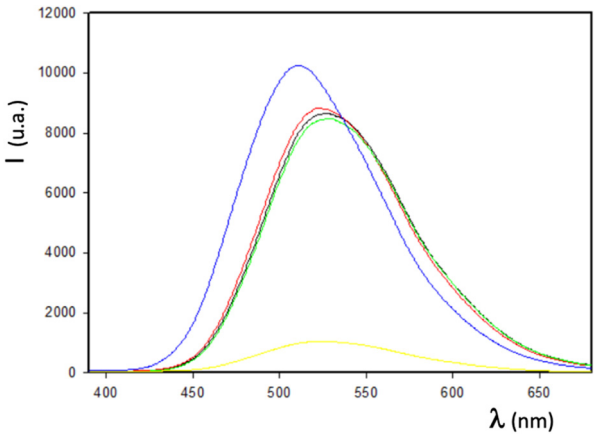

Fig. 3 Fluorescence spectra (λ_{exc} = 350 nm) in CH_3CN/DMSO solution (9 : 1 v/v) of **L1** (black curve), **L2** (red curve), **L3** (green curve), **L4** (yellow curve), and dansylamide (blue curve). The concentration was in all cases 10 μM.

The addition of KET^-, NPX^-, and BzO^- as their sodium salts to all the receptors in CH_3CN/DMSO solution (9 : 1 v/v) does not cause any change in the absorption spectra, except in the case of **L4**. Indeed, the only changes are due to the absorption of the added anion species (for the characteristic absorption spectra of the target guests see Fig. S14 in the ESI†). In the case of **L4**, the addition of guest species causes a pronounced red-shift of the absorption band to 350 nm accompanied by an intensity increase (Fig. 4 in the case of KET^- and Fig. S15 and S16 in the ESI† for NPX^- and BzO^-, respectively). An isosbestic point can be clearly observed in all cases (for naproxen, an equivalent amount of the drug was added to the reference to take into account its absorption) at 330 nm. These changes in the absorption spectra can be attributed to the involvement of the indole units in the HB formation with the guest species, in agreement with what observed in the ^{1}H-NMR studies (see below).

Interestingly, the changes observed in the fluorescence emission are much more relevant. In particular, the macrocyclic receptors **L1** and **L2** show a strong quenching (63% and 71% of the initial value, respectively) upon the addition of

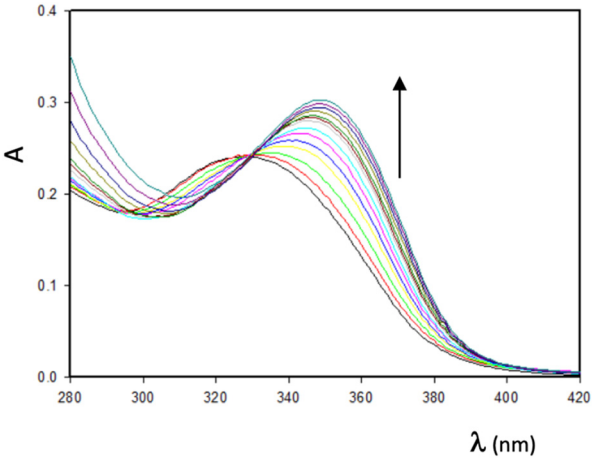

Fig. 4 Absorption spectra in CH_3CN/DMSO solution (9 : 1 v/v) of **L4** (10 μM) upon addition of increasing amounts (0–5 equiv.) of KET^- as its sodium salt.

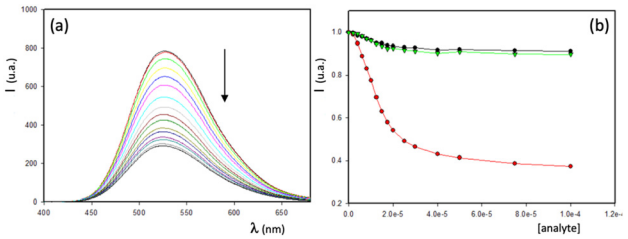

Fig. 5 (a) Fluorescence spectra (λ_{exc} = 350 nm) in CH_3CN/DMSO solution (9 : 1 v/v) of **L1** (10 μM) upon addition of increasing amount of the sodium salt of KET^-; (b) normalized fluorescence intensity (λ_{exc} = 350 nm; λ_{em} = 525 nm) of **L1** (10 μM) upon addition of increasing amount of ketoprofen (red circles), naproxen (green triangles), and benzoate (black circles) as their sodium salt.

KET^-, while their emission remains almost constant upon the addition of NPX^- and BzO^-, as shown in Fig. 5 in the case of **L1** and Fig. S17 in the ESI† in the case of **L2**, respectively.

From the observed quenching, we were able to determine the association constants[23] for the formation of the 1 : 1 adducts with KET^- of both **L1** (9.4×10^4 M^{-1}) and **L2** (8.3×10^4 M^{-1}). Together with the observed intensity decrease, the addition of KET^- led also to a change of the excited state decay. In particular, two different lifetimes – shorter than that measured in absence of the guest (4.5 and 9.0 ns for **L1**; 2.8 and 6 ns for **L2**) – could be observed in the presence of KET^-.

To gain additional insight into the possible interference by other analytes, we performed titration experiments with KET^- also in the presence of BzO^-, obtaining a shift in the titration curve (Fig. 6). This shows that **L1** and **L2** can bind BzO^-, but its presence does not appreciably perturb the photophysical properties of the receptors, indicating that **L1** and **L2** are not selective but sensitive to KET^-.

The two open receptors, **L3** and **L4**, on the contrary, while responding in a similar way to KET^-, with an intensity decrease

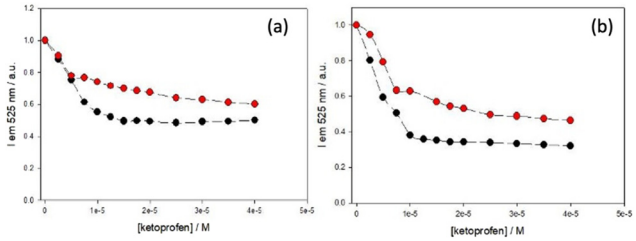

Fig. 6 Trends of emission intensities (λ_{exc} = 350 nm; λ_{em} = 525 nm) in CH_3CN/DMSO solution (9 : 1 v/v) of 10 μM of (a) **L1** and (b) **L2** upon the addition of increasing amount of KET^- in absence (black) and in presence (red) of 10 μM of BzO^-. All the intensities were normalised on the emission of the receptors before any addition of KET^-.

of 56% and 68%, respectively, underwent a drop in the fluorescence intensity also upon the addition of BzO^- and NPX^- (see Fig. S18–S25 in the ESI†). In all cases, the observed quenching of the fluorescence of the dansyl unit is accompanied by a bi-exponential decay of the excited state. The lifetimes are again in all cases shorter than those of free receptors. In the case of **L3** the two observed lifetimes are 12.6 and 4.1 ns after the formation of the adduct with KET^-, 11.8 and 4.0 ns after the addition of BzO^-, and 10.9 and 3.8 ns in case of NPX^-. Interestingly, in the case of KET^-, the highest pre-exponential term (the ratio is *ca.* 1.5) is associated with the shorter lifetime, while in the other two cases the opposite is true (the ratios being 4.5 and 7.5 for BzO^- and NPX^-, respectively), in agreement with the higher quenching observed with KET^- in case of **L4**.

Although it is well known that squaramide receptors could be easily deprotonated by basic anions, the deprotonation was ruled out in our case as demonstrated by the UV-Vis and fluorescence titration performed on **L1** in the presence of tetramethylammonium hydroxide (TBAOH) (see Fig. S26 in the ESI†).

The association constants between the receptors **L1–L4** and the different analytes are gathered in Table 1. In the case of **L1–L3**, in which the absorbance of the receptor does not change during the titration, the constants have been obtained fitting the fluorescence data, while in case of **L4** the association processes have been obtained from the absorption spectra, since following changes in the fluorescence spectra in this case would have caused the need of suitable corrections,[26] increasing the associated errors. Similar values respect to the

Table 1 Association constants (×10^4) for the formation of the 1 : 1 adduct in CH_3CN/DMSO solution (9 : 1 v/v) of **L1–L4** with KET^-, NPX^- and BzO^- as their sodium salts. Results reported as the output of Bindfit[24,25]

	$K_a \times 10^4$ (M^{-1})		
Receptor/analyte	**KET^-**	**NPX^-**	**BzO^-**
L1	9.4 ± 0.6%	n.d.	n.d.
L2	8.3 ± 1%	n.d.	n.d.
L3	7.8 ± 0.3%	8.6 ± 0.3%	2.7 ± 0.7%
L4	16 ± 2.5%	1.6 ± 0.6%	2.3 ± 2.1%

first association constant could however be estimated also from the fluorescence data.

In general, as reported in Table 1, the affinity of **L3** and **L4** for KET^- is similar to those of the macrocyclic squaramides **L1** and **L2** and comparable to that with NPX^-; a slightly lower value has been obtained for BzO^-. Of note, also with these receptors the highest intensity decrease has been observed for KET^-.

These findings demonstrate that, although none of the presented receptors binds ketoprofen selectively, their differential response can allow designing efficient arrays for the determination of polluted samples.[27]

The ability of **L1** to sense ketoprofen as its sodium salt over the other guests was thus tested performing a Strip Test by soaking a paper in a well grinded suspension of the receptors in ethanol. After complete drying, the paper showed, as expected, a blue-green fluorescence under illumination with 360 nm UV lamp. Deposition of aqueous solutions of the guests was then performed (Fig. 7), revealing that the fluorescence is quenched in the case of KET^- and mixed anionic guests, while NPX^- and benzoate have no significant effect. Under these conditions, in order to appreciate the switching-OFF of the fluorescence on the paper strip, substrate concentrations as high as 10^{-3} M, corresponding to about 100 folds the concentration of the sensor, are needed.

^{1}H-NMR titration studies

In order to get an insight on the specific interactions occurring between the receptors and the anion guests and responsible for the optical response described above, ^{1}H-NMR titrations on **L1–L4** using DMSO-d_6/0.5% water as a solvent and the guests as their sodium salts were conducted. In the case of NPX^-, titrations could not be conducted due to solubility issues. All the receptors interacted with KET^- and BzO^- under these experimental conditions (see Fig. S27–S34 in the ESI†).

As shown in the stack-plots in Fig. S27–S32,† in the case of **L1–L3**, the addition of increasing amounts of BzO^- and KET^- caused the broadening of the signals attributed to the squaramide NHs. However, their overlapping with the signals of the guests in the aromatic region, prevented the calculation of reliable association constants.

In the case of **L4** we were able to clearly monitor the downfield shift of the signals attributed to the indole NHs at 11.13 ppm and the one attributed to the squaramide NHs adjacent to the aliphatic chain at 7.95 ppm (although overlapping with the aromatic signals of the receptor, at the beginning of the titration) throughout the titration. Indeed, upon the addition of increasing amounts of BzO^- and KET^- both the signals underwent a dramatic downfield shift ($\Delta\delta$ = 1.72 and 1.89 ppm, respectively, for the titration conducted in the presence of KET^-), suggesting a strong host–guest interaction. However, by fitting the data with a 1 : 1 and 1 : 2 model by using the open source software BindFit,[24,25] we were able to calculate the association constant for the preferential formation of the host–guest adduct with a 1 : 2 stoichiometry.

Fig. 8 shows the stack-plot of the titration of **L4** in the presence of KET^- (the stack plot for the titration with BzO^- is shown in Fig. S34 in the ESI†).

To better understand the behaviour of **L4** in a less competitive medium and to support the spectrophotometric and spectrofluorimetric results, we decided to conduct the ^{1}H-NMR titration also in CD_3CN-d_3/DMSO-d_6 9 : 1 v/v.

As shown in the stack-plot reported in Fig. S35 and S36,† a behaviour similar to that described above for the titrations conducted in DMSO-d_6/0.5% water, was observed. However, it is worth noticing that in this experimental condition, the fitting of the data allowed us to calculate the association constants for the formation of the 1 : 1 host–guest adduct (in agreement with those obtained by spectrophotometric and spectrofluorimetric studies), suggesting a strong solvent dependence of the stoichiometry of the adducts formed by **L4** with the target anions.

It is worth noticing that a deprotonation process could be ruled out as demonstrated by the titration conducted for the macrocyclic squaramide **L1** and the open chain squaramide **L4** in the presence of TBAOH (see Fig. S37 and S38 in the ESI†), in which the NH signals completely disappeared upon the addition of 2 equivalents of the base with respect to both the receptors.

Theoretical calculations

Calculations were carried out at the Density Functional Theory (DFT)[28–31] level in order to investigate the structural and energetic features of the interactions between the dansylate squara-

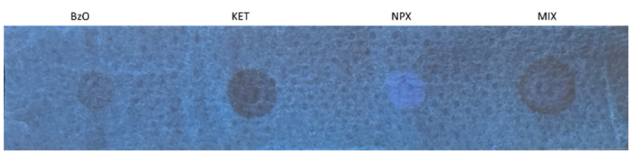

Fig. 7 Strip-test of **L1** with addition of naproxen, ketoprofen, benzoate and three guests mixed (illumination at 360 nm).

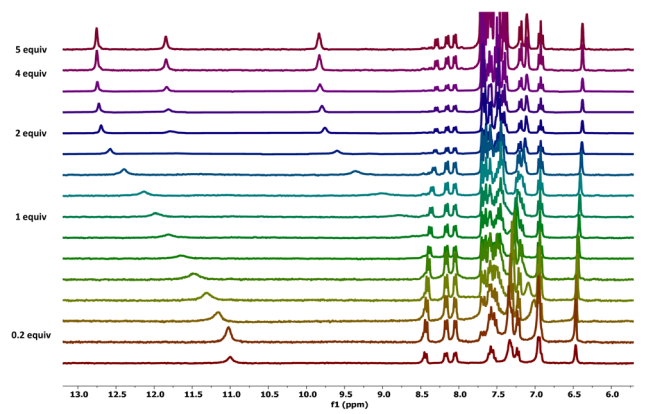

Fig. 8 Stack plot of the ^{1}H-NMR titration of **L4** (5.0×10^{-3} M) in DMSO-d_6/0.5% water at 298 K in the presence of increasing molar ratios of KETNa (0.075 M).

mide-based receptors and the anionic forms of the investigated anti-inflammatory drugs. DFT calculations were proved to be particularly well-suited for probing intermolecular interactions involving hydrogen bonds (HB),[32,33] halogen bonds (XB),[34,35] and chalcogen bonds (ChB),[36–38] providing excellent results, comparable with those achieved by post-HF perturbative methods, at an affordable computational cost. Following the very encouraging computational results obtained for related systems featuring XH and XB interactions,[17,39,40] the mPW1PW functional[41] was used along with the Def2SVP basis sets[42] for all atomic species.

BzO^- and KET^- were chosen as model anions. For both anions the geometry was optimized (see Fig. S40 in the ESI†) providing a very good agreement between the available structural data and the optimized metric parameters.[43] A TD-DFT investigation revealed a very weak absorption peak at about 280 nm (monoelectronic transitions at 4.339 and 4.418 eV; f = 0.006 and 0.009, respectively) for the benzoate anion and a broad band in the region 250–350 nm for the KET^- anion, due to the contribution of monoelectronic transitions calculated at 287, 332, and 335 nm (4.325, 3.737, and 3.698 eV; f = 0.164, 0.038, and 0.047, respectively).

As model squaramide-based chemosensors, receptors **L2** and **L4** were chosen (see Fig. S41 in the ESI†). The absorption spectrum simulated for **L2** based on TD-DFT calculations (see Fig. S42 in the ESI†) shows a weak absorption at 371 nm (3.34 eV; f = 0.088), due to the HOMO–LUMO monoelectronic excitation, and a series of absorptions at about 250 nm resulting in a structured peak, mainly contributed by the allowed singlet vertical transition from the ground state (GS) to the manifold of excited state (ES) ranging between ES #13 and ES #31. The most intense of these transitions is the GS → ES #27 vertical transition (4.98 eV; f = 0.341), due to a monoelectronic excitation localized on the squaramide core. Notably, TD-DFT data are in very good agreement with the experimental absorption spectrum recorded for **L2** (Fig. 2), showing the main absorption maximum at 4.35 eV. The absorption spectrum simulated for **L4** based on TD-DFT calculations (see Fig. S43 in the ESI†) shows a main peak bathochromically shifted with respect to that calculated for **L2**, in agreement with UV-Vis spectroscopic measurements, and attributed to the singlet electronic vertical transition from the GS to the ES #11 (4.081 eV; f = 0.504). This transition is mainly contributed by two monoelectronic excitation localized on the indol-7-yl substituent (KS-MO 204 → 208) and the squaramide core (KS-MO 206 → 210).

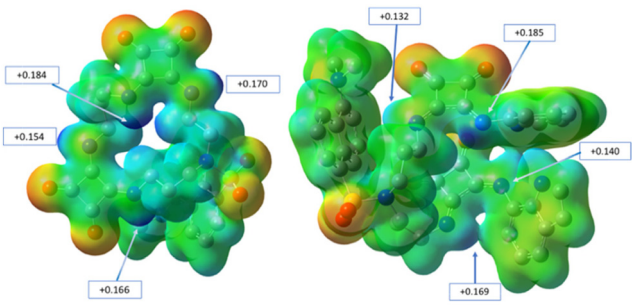

Fig. 9 Molecular electrostatic potential (MEP) mapped on the electron densities (0.01 |e| per $Bohr^3$) for **L2** (left) and **L4**. Range −0.10 (red) to +0.18 (blue) a.u.

As expected, the maps of the electrostatic potential calculated for BzO^-, KET^-, **L2**, and **L4** show the most negative potential on the carboxylate endings of the anions, and the most positive potentials on the squaramide NH groups of **L2** and **L4** (Fig. 9), suggesting that the electrostatic interaction may drive the anions to interact with receptors by means of HB interactions, in agreement with ^{1}H-NMR experiments (see above).

The 1 : 1 adducts between the receptors **L2** and **L4** and the anions BzO^- and KET^- were singly optimized to investigate the receptor–anion interactions. For each adduct several stable geometries were obtained, summarised in Table 2 (entries a–j; see Fig. S44 in the ESI†) and Fig. 10 for **L4**·KET^- in its most stable optimized geometry.

In general, the $-COO^-$ group of the anions can either form two HB interactions with the two NH of a single squaramide or bridge two squaramide systems by forming two bifurcated HBs. Depending on the final geometry, the indole N–H group

Table 2 Total electronic energies (E, Hartree), maximum absorption wavelength (λ_{max}, nm)[a] and relevant molar extinction coefficient (ε, 10^3 M^{-1} cm^{-1}),[a] adduct stabilization energies (ΔE, kcal mol^{-1}) and type of HB in the adducts a–j between the receptors **L2**/**L4** and the anions BzO^-/KET^- optimized at DFT level

Entry	Adduct	E	λ_{max}[a,b]	ε	ΔE	Main interactions
a	**L2**·BzO^-	−2721.4923	258	40	62.25	2 HB
b		−2721.5026	258	47	**68.68**	2 bifurc. HB
c	**L2**·KET^-	−3144.0988	256	53	60.38	2 HB
d		−3144.1090	256	56	**66.75**	2 bifurc. HB
e	**L4**·BzO^-	−3329.4688	318	33	58.39	2 HB
f		−3329.4986	324	52	77.06	2 bifurc. HB + 1 intramol. HB
g		−3329.4996	323	47	**77.75**	2 bifurc. HB + 2 ind.[c] HB
h	**L4**·KET^-	−3752.0799	309	24	59.43	2 HB
i		−3752.1047	324	52	**74.96**	2 bifurc. HB + 1 intramol. HB[c]
j		−3752.1030	324	46	73.92	2 bifurc. HB + 2 ind.[c] HB

[a] λ_{max} and ε value obtained from the convolution of the electronic excitations assuming a half-bandwidth of 0.333 eV. [b] λ_{max} = 249 and 304 nm for **L2** and **L4**, respectively. [c] HB involving the NH indole group.

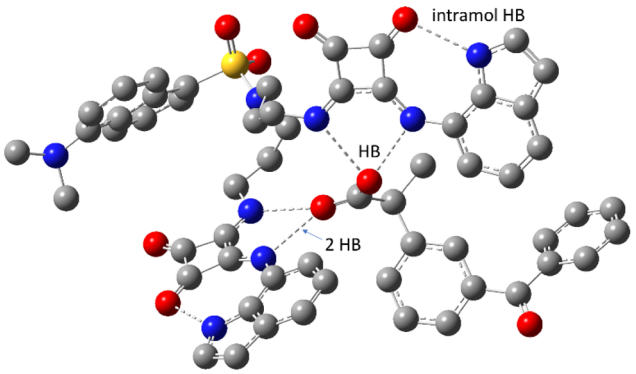

Fig. 10 Optimized geometry of the most stable 1 : 1 adduct **L4**·KET$^-$ (entry i in Table 2). The bifurcated hydrogen bonds as well as the intramolecular HB within **L4** were evidenced. Hydrogen atoms were omitted for clarity.

can interact with a C=O of the bonded squaramide or even further strengthen the interaction with the anion with an additional intramolecular HB. Notably, the total electronic energies calculated for adducts of the same stoichiometry are marginally affected by the type and number of HBs formed. In general, the interaction of the anions with the receptor **L4** provides a larger stabilization than those formed by **L2**.

The absorption of the receptor in the adducts has been evaluated at TD-DFT level (Table 2).

In general, the interaction of **L2** and **L4** with both anions results in a bathochromic shift (by 20 nm in the gas phase) accompanied by an hyperchromic effect, both effect increasing with the number of HB interactions occurring between the receptor and the anion. Therefore, the red-shift of the receptor absorption band and the increase in the molar extinction coefficients observed because of the receptor-anion interaction, represent possible parameters for the evaluation of the sensing ability of the tested receptors towards specific anions.

Moreover, the flexibility of the open chain squaramide **L4** also allows the formation of host–guest adducts with both BzO$^-$ and KET$^-$ with a 1 : 2 stoichiometry (see ESI for detailed discussions†). All these findings perfectly support all the results obtained with different spectroscopic techniques.

Conclusions

This study describes the behaviour of four fluorescent squaramide-based receptors providing a guideline for the realization of chemosensors suitable for the sensing of organic carboxylic anions, such as NSAID derivatives, which can be included in the Emerging Pollutants list. It is worth noticing that no examples of squramide-based fluorescent receptors for the recognition of these important targets have been reported so far in the literature. In particular, the paper reports four receptors containing the *N*,*N*-bis(3-squarmidoylpropyl)dansylamide motif (SQ-CH_2-CH_2-CH_2)$_2$N-DNS as fluorescent receptive unit inserted in two macrocycles (**L1** and **L2**) and two open-chain systems (**L3** and **L4**).

As demonstrated by ^{1}H-NMR, UV-Vis and fluorescence studies, all receptors interact with the selected guests (ketoprofen, naproxen and benzoic acid as sodium salts) in organic solvents. Notably, only the macrocyclic systems **L1** and **L2** show a specificity in the fluorescence response to ketoprofen. In fact, while the open-chain receptors **L3** and **L4** undergo a quenching of the fluorescence upon addition of ketoprofen, naproxen and benzoate as their sodium salts, the macrocyclic systems **L1** and **L2** were quenched only by ketoprofen. This aspect highlights the role of the highly organised macrocyclic structure in improving the specificity and/or the selectivity of a chemosensor. The ability of **L1** to discriminate between ketoprofen and the other examined guests was also confirmed using a strip-test able to work in water.

Theoretical calculations performed on receptors **L2** and **L4** at DFT level confirm that the stabilization of the adducts with ketoprofen and benzoate is mediated by H-bond interactions between the squaramidic and/or indolic NH groups (HB donors) of the hosts and the carboxylate groups of the guests. However, the macrocyclic backbone balances the more HB contacts of **L4** resulting in similar K_{ass} values.

Summarizing the results of these studies, it can be deduced that the pre-organization and the number of H-bond donor sites are the two main factors that should be considered in order to design receptors able to respond to a specific anion. Moreover, the possibility to realize chemosensors with different response can allow for the design of efficient arrays for the determination of polluted samples.

Author contributions

Conceptualisation: C. C., L. P., V. F. Data curation: G. P., L. M., F. I., L. M. (Liviana Mummolo), L. G., M. F. Investigation: G. P., L. M., F. I., L. M. (Liviana Mummolo), L. G., M. F., M. A. Supervision: C. C., L. P., V. F. Writing (original draft): C. C., L. G., G. P., L. P., M. A., L. M. (Liviana Mummolo), V. F. Writing (reviewing ad editing): all authors. Funding acquisition: C. C., L. P., V. F. Validation: all authors.

Conflicts of interest

There are no conflicts to declare.

Acknowledgements

Financial support from MIUR (PRIN 2017 project 2017EKCS35) is gratefully acknowledged. C. C., V. L., M. A., M. C. M. thank Università degli Studi di Cagliari (FIR 2016–2019), Fondazione di Sardegna (FdS Progetti Biennali di Ateneo, annualità 2020) for financial support. We would like to thank CeSAR for NMR facilities.

References

1 P. E. Rosenfeld and L. G. H. Feng, *Risks of Hazardous Wastes*, ed. P. E. Rosenfeld and L. G. H. Feng, William Andrew Publishing, Boston, 2011, pp. 215–222.
2 V. Geissen, H. Mol, E. Klumpp, G. Umlauf, M. Nadal, M. van der Ploeg, S. E. A. T. M. van de Zee and C. J. Ritsema, *Int. Soil Water Conserv. Res.*, 2015, **3**, 57–65.
3 N. Z. Arman, S. Salmiati, A. Aris, M. R. Salim, T. H. Nazifa, M. S. Muhamad and M. Marpongahtun, *Water*, 2021, **13**, 3258.
4 A. Rastogi, M. K. Tiwari and M. M. Ghangrekar, *J. Environ. Manage.*, 2021, **300**, 113694.
5 A. L. Moreno Ríos, K. Gutierrez-Suarez, Z. Carmona, C. G. Ramos and L. F. Silva Oliveira, *Chemosphere*, 2022, **291**, 132822.
6 D. Smiljanić, B. de Gennaro, F. Izzo, A. Langella, A. Daković, C. Germinario, G. E. Rottinghaus, M. Spasojević and M. Mercurio, *Microporous Mesoporous Mater.*, 2020, **298**, 110057.
7 F. Caroleo, G. Magna, M. L. Naitana, L. Di Zazzo, R. Martini, F. Pizzoli, M. Muduganti, L. Lvova, F. Mandoj, S. Nardis, M. Stefanelli, C. Di Natale and R. Paolesse, *Sensors*, 2022, **22**, 2649.
8 R. H. Farahi, A. Passian, L. Tetard and T. Thundat, *ACS Nano*, 2012, **6**, 4548–4556.
9 G. M. Romano, L. Mummolo, M. Savastano, P. Paoli, P. Rossi, L. Prodi and A. Bencini, *Chem. Commun.*, 2022, 7022–7025.
10 A. Akdeniz, L. Mosca, T. Minami and P. Anzenbacher, *Chem. Commun.*, 2015, **51**, 5770–5773.
11 L. A. Marchetti, L. K. Kumawat, N. Mao, J. C. Stephens and R. B. P. Elmes, *Chem*, 2019, **5**, 1398–1485.
12 R. I. Storer, C. Aciro and L. H. Jones, *Chem. Soc. Rev.*, 2011, **40**, 2330–2346.
13 R. Prohens, S. Tomàs, J. Morey, P. M. Deyà, P. Ballester and A. Costa, *Tetrahedron Lett.*, 1998, **39**, 1063–1066.
14 S. Tomàs, R. Prohens, M. Vega, M. C. Rotger, P. M. Deyà, P. Ballester and A. Costa, *J. Org. Chem.*, 1996, **61**, 9394–9401.
15 J. I. Lachowicz, G. Picci, P. Coni, V. Lippolis, M. Mamusa, S. Murgia, G. Pichiri and C. Caltagirone, *New J. Chem.*, 2019, **43**, 10336–10342.
16 G. Picci, M. Kubicki, A. Garau, V. Lippolis, R. Mocci, A. Porcheddu, R. Quesada, P. C. Ricci, M. A. Scorciapino and C. Caltagirone, *Chem. Commun.*, 2020, **56**, 11066–11069.
17 G. Picci, J. Milia, M. C. Aragoni, M. Arca, S. J. Coles, A. Garau, V. Lippolis, R. Montis, J. B. Orton and C. Caltagirone, *Molecules*, 2021, **26**, 1301.
18 G. Ambrosi, M. Formica, V. Fusi, L. Giorgi, A. Guerri, M. Micheloni, P. Paoli, R. Pontellini and P. Rossi, *Chem. – Eur. J.*, 2007, **13**, 702–712.
19 G. Ambrosi, M. Formica, V. Fusi, L. Giorgi, E. MacEdi, M. Micheloni, P. Paoli, R. Pontellini and P. Rossi, *Chem. – Eur. J.*, 2011, **17**, 1670–1682.
20 L. Qin, J. R. Wright, J. D. E. Lane, S. N. Berry, R. B. P. Elmes and K. A. Jolliffe, *Chem. Commun.*, 2019, **55**, 12312–12315.
21 M. A. Ilies, W. A. Seitz, B. H. Johnson, E. L. Ezell, A. L. Miller, E. B. Thompson and A. T. Balaban, *J. Med. Chem.*, 2006, **49**, 3872–3887.
22 J. E. Richman and T. J. Atkins, *J. Am. Chem. Soc.*, 1974, **96**, 2268–2270.
23 D. Genovese, M. Cingolani, E. Rampazzo, L. Prodi and N. Zaccheroni, *Chem. Soc. Rev.*, 2021, **50**, 8414–8427.
24 D. Brynn Hibbert and P. Thordarson, *Chem. Commun.*, 2016, **52**, 12792–12805.
25 P. Thordarson, *Chem. Soc. Rev.*, 2011, **40**, 1305–1323.
26 A. Credi and L. Prodi, *J. Mol. Struct.*, 2014, **1077**, 30–39.
27 D. G. Smith, I. L. Topolnicki, V. E. Zwicker, K. A. Jolliffe and E. J. New, *Analyst*, 2017, **142**, 3549–3563.
28 K. Burke and L. O. Wagner, *Int. J. Quantum Chem.*, 2013, **113**, 96–101.
29 W. Kohn and L. J. Sham, *Phys. Rev.*, 1965, **140**, A1133–A1138.
30 P. Makkar and N. N. Ghosh, *RSC Adv.*, 2021, **11**, 27897–27924.
31 W. Koch, M. C. Holthausen, *A Chemist's Guide to Density Functional Theory*, 2nd edn, 2001.
32 J. S. Arey, P. C. Aeberhard, I. C. Lin and U. Rothlisberger, *J. Phys. Chem. B*, 2009, **113**, 4726–4732.
33 A. D. Boese, *ChemPhysChem*, 2015, **16**, 978–985.
34 S. Kozuch and J. M. L. Martin, *J. Chem. Theory Comput.*, 2013, **9**, 1918–1931.
35 A. Siiskonen and A. Priimagi, *J. Mol. Model.*, 2017, **23**, 50.
36 C. Bleiholder, D. B. Werz, H. Köppel and R. Gleiter, *J. Am. Chem. Soc.*, 2006, **128**, 2666–2674.
37 A. P. M. Arca and G. Ciancaleoni, *Chalcogen Chemistry: Fundamentals and Applications*, ed. C. S. Vito Lippolis, E. J. Lenardão and A. L. Braga, RSC, 2023.
38 W. Wang, B. Ji and Y. Zhang, *J. Phys. Chem. A*, 2009, **113**, 8132–8135.
39 M. C. Aragoni, M. Arca, F. A. Devillanova, F. Isaia and V. Lippolis, *Cryst. Growth Des.*, 2012, **12**, 2769–2779.
40 R. Montis, M. C. Aragoni, M. Arca, S. J. Coles, V. Lippolis, J. Milia, J. B. Orton, L. Pala, G. Picci, T. Pivetta and C. Caltagirone, *Eur. J. Inorg. Chem.*, 2021, **2021**, 3878–3885.
41 C. Adamo and V. Barone, *J. Chem. Phys.*, 1998, **108**, 664–675.
42 F. Weigend and R. Ahlrichs, *Phys. Chem. Chem. Phys.*, 2005, **7**, 3297–3305.
43 P. Rossi, P. Paoli, L. Chelazzi, S. Milazzo, D. Biagi, M. Valleri, A. Ienco, B. Valtancoli and L. Conti, *Cryst. Growth Des.*, 2020, **20**, 226–236.